Colloids and Surfaces B: Biointerfaces 180 (2019) 429–440

Contents lists available at ScienceDirect

Colloids and Surfaces B: Biointerfaces

journal homepage: www.elsevier.com/locate/colsurfb

Amphipathic β-cyclodextrin nanocarriers serve as intelligent delivery platform for anticancer drug

Hui Liu, Jian Chen, Xiufang Li, Zhiwei Deng, Peiru Gao, Jianbin Li, Tao Ren, Ling Huang, Yanjing Yang*, Shian Zhong*

College of Chemistry and Chemical Engineering, Central South University, Changsha, Hunan, 410083, PR China

ARTICLE INFO

Keywords:
Antitumor drug
Amphiphilic β-CD
GSH-responsiveness
Drug loading

ABSTRACT

A novel glutathione-responsive (GSH-responsive) star-like amphiphilic polymer $(C_{12}H_{25})_{14}$-β-CD-(S-S-mPEG)$_7$ (denoted as CCSP) was designed for efficient antitumor drug delivery. The amphiphilic β-cyclodextrin (β-CD) self-polymerize in water to form a sphere with a diameter of 40–50 nm. The secondary hydroxyl groups of β-CD were modified by dodecyl to form a hydrophobic core and the primary hydroxyl groups of β-CD were decorated with PEG through disulfide bond to form a hydrophilic shell. Since the hydrophobic cavity of β-CD was maintained, the hydrophobic core formed by dodecyl as well as cavity of β-CD provided CCSP with a loading content as high as 39.6 wt%. Importantly, DOX@CCSP exhibited low drug leakage and negligible cytotoxicity in non-reductive physiological environment, while it showed rapid release and high cytotoxicity in reductive tumorous environment *via* the breakage of disulfide bond. In view of the above-mentioned advantages of DOX@CCSP nanocarriers such as high loading content, proper size, favorable stimulus-response release performance and low leakage, it is believed that CCSP may offer great potential to be used as an intelligent nanocarrier for anticancer drug delivery.

1. Introduction

Today, cancer represents a disease with the highest mortality rate [1]. However, currently available clinical chemotherapeutic agents are subjected to common shortcomings including high toxicity, short half-live and low selectivity [2]. Therefore, it is particularly important to develop new technologies to improve anticancer efficiently. With the development of nanotechnology, nanocarriers have been gaining more and more attention in the scientific community partially due to the large surface area, appropriate size and unique structure [3–5]. These characteristics made it particularly suitable for serving as drug carrier with the advantages of prolonging blood circulation [6], and accumulation in tumor tissues benefiting from the enhanced permeability and retention effect (EPR effect) [7,8]. However,severe side effects are mainly caused by no selectivity of anticancer drug between tumor tissues and healthy tissues. Moreover, premature drug leakage from drug carriers is often observed during blood circulation in the body [9,10], and drug loading is also a critical aspect when drug delivery systems (DDS) was designed [11]. Therefore, drug leakage during blood circulation need to be decreased and the drug loading content need to be improved when DDS was used *in vivo*. Moreover, the stimulus-responsive release in tumor tissues is another critical aspect that needs to be addressed.

There are various differences in the microenvironment between tumor cells and normal cells, such as temperature [12,13], pH [14,15] and content of reduced glutathione (GSH) [16,17]. These differences provide a theoretical basis for the design of stimulus-responsive nanocarriers. β-CD represents a type of natural compound which proves to be nontoxic, biocompatible and biodegradable. There is a hydrophobic cavity and a hydrophilic shell in β-CD [18], which renders the material suitable to be used as drug carrier. Moreover, There are 21 hydroxyl groups at two ends of β-CD, which make it easy to modify [19,20]. However, poor water solubility and low drug loading content of β-CD limit its further development. At present, polyethylene glycol (PEG) is most commonly used as hydrophilic material to decorate particulate surfaces since its advantages: increasing water solubility, avoiding recognition by cells of the mononuclear phagocyte system (MPS) [21], prolonging blood circulation and nontoxicity. Based on the above case, β-CD was modifiedwith hydrophilic (PEG) and hydrophobic (dodecyl) groups to form amphipathic nanocarriers for loading chemotherapy drugs. Then, water solubility as well as the drug loading content could be increased, in addition, the stimulus-responsive bonds were

* Corresponding authors.
E-mail addresses: yangyanjing@csu.edu.cn (Y. Yang), zhongshian@aliyun.com (S. Zhong).

https://doi.org/10.1016/j.colsurfb.2019.05.011
Received 6 January 2019; Received in revised form 17 April 2019; Accepted 7 May 2019
Available online 08 May 2019
0927-7765/

introduced into the DDS to endow the material with a stimulus-responsive control release behavior.

In general, amphipathic β-CD is constructed by host-guest interaction in the previous studies [22–24]. Whereas amphipathic β-CD was synthesized by chemical bonding so as to retain the nature cavity of β-CD and increase the drug loading content. Herein, a novel amphiphilic star-like copolymer as DDS based on β-CD derivatives was prepared in this work. First, the primary hydroxyl groups of β-CD were protected. Then, the secondary hydroxyl groups of β-CD were modified with bromododecane to form hydrophobic ends. Next, bromine was grafted into the primary hydroxyl groups of β-CD upon addition of Br_2. Sulfydryl was then introduced into the primary hydroxyl groups of β-CD and the final product was reacted with PEG-SH to form CCSP. It is noteworthy that amphiphilic β-CD could self-polymerize in water to form spherical polymers. The dodecyl groups acted as a hydrophobic core and polyethylene glycol groups served as hydrophilic shell, where the cavity of β-CD and the hydrophobic cavity after self-assembly provided a suitable area to entrap DOX with a drug loading content as high as 39.6 wt%. Disulfide bonds are known to be reduction-sensitive chemical bonds and it was demonstrated that DOX could be released from DOX@CCSP by disulfide bond dissociation in a reductive tumor environment. It showed that DOX@CCSP could selectively kill cancerous SKOV3 cells but showed low toxicity towards normal HEK 293T cells. Moreover, because DOX@CCSP could selectively accumulate and release in the tumor tissues, it demonstrated a beneficial anticancer effect with low toxicity to normal tissues in nude mice (Fig. 1).

2. Experimental section

2.1. Materials and reagents

Chemical reagents including 1-bromododecane, anhydrous pyridine, methoxypolyethylene glycol (mPEG, M_n = 2 kDa), β-cyclodextrin (β-CD), *tert*-butyldimethylsilyl chloride (TBDMS-Cl), triphenylphosphine (Ph_3P), DL-1,4-dithiothreitol (DTT), and doxorubicin hydrochloride (DOX) were purchased from Energy Chemical Technology Co. Ltd (Shanghai, China) or Aladdin Chemical Technology Co. Ltd (Shanghai, China). Fetal bovine serum (FBS), Dulbecco's modified eagle medium (DMEM), and Phosphate buffered saline (PBS) were purchased from Beyotime Biotechnology Co. Ltd (Hunan, China). *N,N*-Dimethylformamide (DMF), dimethylsulfoxide (DMSO) and dichloromethane (DCM) were distilled over calcium hydride (CaH_2) to remove any residual moisture before use. Other reagents were commercially available and usedwithout further purification.

2.2. Characterization

^{1}H NMR spectra were operated on a 400 MHz or 500 MHz NMR spectrometer (Bruker, Germany) and the internal standard was tetramethylsilane (TMS). The average size of micelles was obtained using dynamic light scattering (DLS) through Zetasizer Nano-ZS from Malvern Instruments equipped with a 633 nm He-Ne laser using backscattering detection. The molecular weight and mass distribution of CCSP and CSP were determined by a Perkin-Elmer Series-200 gel permeation chromatograph (GPC) instrument equipped with PLgel 5 μm Mixed 2D columns. Fourier transform infrared spectrometric (FTIR) analysis was carried out on a Nicolet iS5 Fourier transform infrared spectrometer (USA). Morphology images were obtained using transmission electron microscopy (TEM) and energy dispersive spectrometric (EDS) data of the synthetic micelles were obtained on a JEOL-2100F instrument (Japan). Fluorescence images were obtained on an Operetta High-Content Imaging System (PerkinElmer). The flow cytometer used throughout the studies was purchased from Beckman Coulter Co. Ltd(USA). The DOX contents in tissues were detected using high performance liquid chromatography (HPLC) (Agilent 1260, USA). Biodistribution analysis of DOX in nude mice was obtained using an IVIS Lumina II multispectral imaging system (Caliper Life Sciences, USA).

2.3. Synthesis of per-6-tert-butyldimethysilyl-β-cyclodextrins [β-CD-(OTBDMS)$_7$]

To ensure the successful synthesis of amphiphilic β-CD, hydroxyl groups in the primary face of β-CD featuring high reactivity, had to be

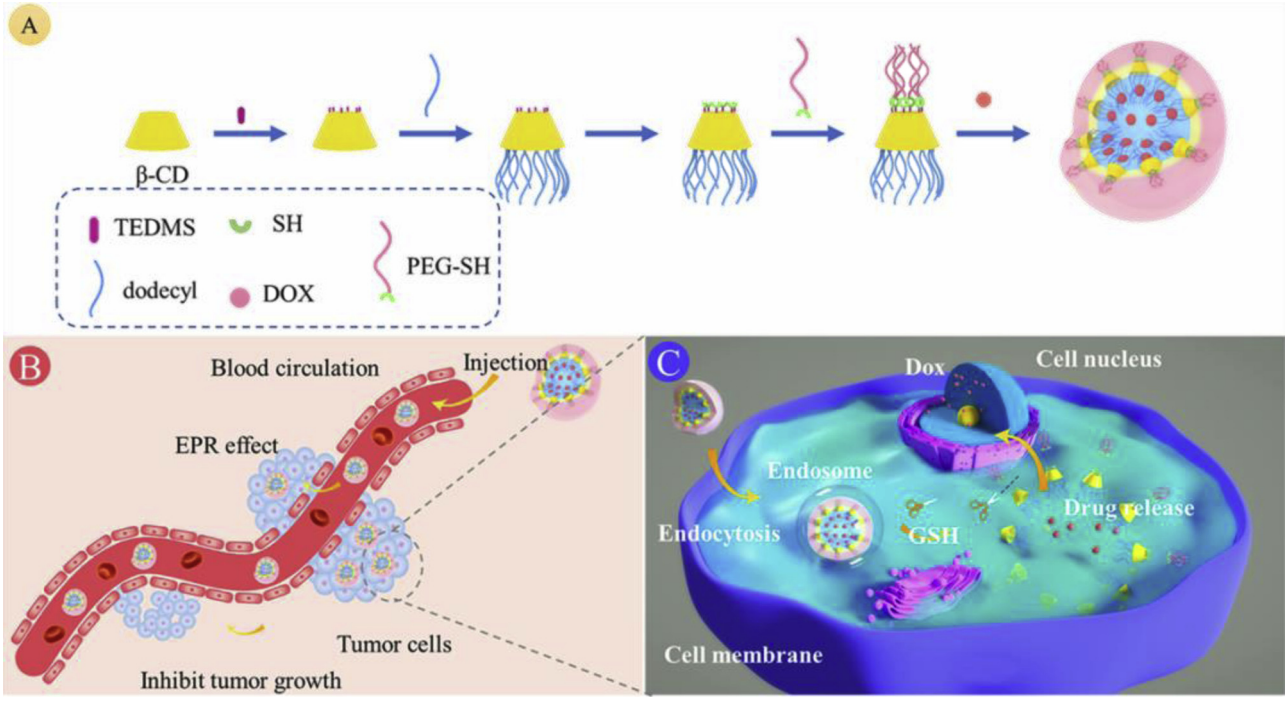

Fig. 1. (A) Schematic illustration highlighting the preparation of amphipathic DOX-loaded β-CD material; (B) Controlled release of DOX in blood circulation; (C) Controlled release of DOX in tumor cells.

protected. *Tert*-butyldimethylsilyl chloride, a widely used protective group for primary hydroxyl groups, was selected to protect the hydroxyl groups [25,26]. The preparation method for β-CD-(OTBDMS)$_7$ comprise the following steps, firstly, dry β-CD (9 g, 7.93 mmol) was dissolved in anhydrous pyridine (100 mL) with constant stirring under argon atmosphere. And the resulting mixture was cooled to 0 °C before *tert*-butyldimethylsilyl chloride (14.5 g, 96.2 mmol) was added dropwise over 3.5 h. The reaction was continued for another 3 h at 0 °C before it was warmed to room temperature for a further 24 h. Then, the pyridine was removed under reduced pressure to provide a milky white powder. The powder was then dissolved in dichloromethane and treated with $KHSO_4$ (aqueous solution) to remove the remaining pyridine. The organic phase was then washed with saturated NaCl aqueous solution and deionized water, dried over anhydrous Na_2SO_4. Dichloromethane was removed *in vacuo* and per-6-*tert*-butyldimethysilyl-β-CD (yield: 86.3%) was obtained *via* recrystallization from MeOH/$CHCl_3$ (95:5, V/V).

2.4. Synthesis of per-[6-(tert-butyldimethylsilyl)-6-deoxy] -per-2,3-dodecyl-β-cyclodextrin [($C_{12}H_{25}$)$_{14}$-β-CD-(OTBDMS)$_7$]

(1) NaH (0.5 g, 20.83 mmol) was placed in a three-neck flask. Then, anhydrous hexane was added to wash the extra kerosene on the NaH solid. (2) Anhydrous THF/DMF (1:1, V/V, 80 mL) was added and the suspension was cooled to 0 °C before β-CD-(OTBDMS)$_7$ (1 g, 0.52 mmol) in anhydrous THF/DMF (1:1, V/V, 20 mL) was added by slow dripping. (3) The reaction was allowed to proceed for 0.5 h at 0 °C before warmed to room temperature for a further 24 h. (4) 1-Bromododecane (7.3 mL, 15.44 mmol) was added dropwise. (5) The reaction was allowed to proceed in the dark for 4 days. (6) Additional NaH (0.5 g, 20.83 mmol) was introduced carefully with cooling. (7) Steps (3), (4), and (5) were repeated once. (8) MeOH was added at 0 °C to quench excess NaH until no more molecular hydrogen (bubbles) was produced. (10) The solvent mixture was removed under reduced pressure and the crude product was dissolved in dichloromethane. The dichloromethane layer was washed with deionized water until the aqueous phase became neutral and the organic phase was then dried over anhydrous Na_2SO_4. Dichloromethane was removed to obtain a gray solid which was purified by glucan gel chromatography with MeOH as an eluant. A yellowish oily substance (1.19 g, yield: 54.1%) was obtained.

2.5. Synthesis of per-(6-bromo-6-deoxy)-per-2,3-dodecyl-β-cyclodextrin [($C_{12}H_{25}$)$_{14}$-β-CD-Br$_7$]

The reaction was carried out according to a procedure reported in the literature [27]. In a general synthesis and under argon atmosphere, PPh_3 (0.67 g, 2.55 mmol) was dissolved in dry dichloromethane (10 mL). After the reaction system was cooled to 0 °C, Br_2 (2.52 mL, 1 mol/L Br_2-CH_2Cl_2) was added by slow dripping. Then, per-[6-(*tert*-butyldimethylsilyl)-6-deoxy]-per-2,3-dodecyl-β-CD (1.44 g, 0.34 mmol, dissolved in 4 mL dry dichloromethane) was added and the reaction proceeded at room temperature for 36 h. The dichloromethane layer was washed by saturated $NaHCO_3$ aqueous solution and deionized water. The organic phase was combined and dried over anhydrous Na_2SO_4. Dichloromethane was removed and the residue was purified by glucan gel chromatography with MeOH as an eluant to obtain a yellow substance (0.91 g, yield: 68.3%).

2.6. Synthesis of per-(6-thiol-6-doexy)-per-2,3-dodecyl-β-cyclodextrin [($C_{12}H_{25}$)$_{14}$-β-CD-(SH)$_7$]

The reaction was carried out according to a procedure reported in the literature [28]. In a general synthesis and under argon atmosphere, synthetic ($C_{12}H_{25}$)$_{14}$-β-CD-Br$_7$ (3.10 g, 0.79 mmol) and thiourea (0.93 g, 12.20 mmol) were dissolved in dry DMF (40 mL) and the reaction proceeded at 70 °C for 24 h. Afterwards, half of the DMF was removed under reduced pressure and NaOH (0.13 g, 3.25 mmol, aqueous solution) was added. The reaction system was then refluxed for 1.5 h before allowed to cool down to room temperature. The pH of the resulting suspension was adjusted with $KHSO_4$ solution until pH < 7, extracted with dichloromethane, and dried over anhydrous Na_2SO_4. Dichloromethane was removed and the crude product was purified by glucan gel chromatography with MeOH as an eluant to obtain a light yellow product (2.1 g, yield: 74.0%).

2.7. Synthesis of amphiphilic β-cyclodextrins [($C_{12}H_{25}$)$_{14}$-β-CD-(S-S-mPEG)$_7$ abbreviated as CCSP]

Synthetic ($C_{12}H_{25}$)$_{14}$-β-CD-(SH)$_7$ (0.20 g, 0.055 mmol) and synthetic mPEG-SH (0.78 g, 0.39 mmol, see Supporting information section) were dispersed in DMSO (10.0 mL) and H_2O_2 (0.4 mL, 30%) was added dropwise. The reaction proceeded at room temperature for 24 h. Deionized water (50 mL) was added dropwise with gentle stirring for 24 h. The mixture was then dialyzed (MWCO 3500) against deionized water for 3 days and lyophilized. A fluffy white product (0.45 g, yield: 45.9%) was obtained.

2.8. Synthesis of amphiphilic β-cyclodextrins [β-CD-(S-S-mPEG)$_7$ abbreviated as CSP] as control materials

The synthetic procedure to produce β-CD-(S-S-mPEG)$_7$ included iodination of hydroxyl groups in the primary face of β-CD, thiolation and thiol oxidation procedures were described in the SupportingInformation section.

2.9. Synthesis of amphiphilic β-cyclodextrin nanocarriers loaded doxorubicin [CCSP@DOX or CSP@DOX] and assessment of drug loading performance

The model drug DOX·HCl (20 mg) was dispersed in DMSO (2 mL), and trimethylamine (10.64 μL) was added to neutralize HCl. The color of the solution slowly turned deep purple from the initial red after the mixture was stirred in the dark overnight. CCSP or CSP (20 mg) was added and the resulting mixture was allowed to stir for 3 h. Then, deionized water (10 mL) was added dropwise, followed by gentle stirring for another 24 h. Then, the mixture was dialyzed (MWCO 3500) against deionized water for 3 days and the mixture was lyophilized. In doing so, a fluffy red product DOX@CCSP (19 mg) or DOX@CSP (15 mg) was obtained.

To determine the loading content of DOX@CCSP or DOX@CSP, the DOX@CCSP or DOX@CSP (1 mg) was dissolved in MeOH (5 mL) with ultrasound aid and a UV spectrum was recorded at 490 nm. The loading content (LC%) of DOX was measured using the following equation:

$$LC\% = \frac{\text{quality of drug in nanocarriers}}{\text{quality of drug and nanocarriers}} \times 100$$

The reductive environment in tumor tissue was simulated by addition of dithiothreonol (DTT). The *in vitro* release behavior of DOX@CCSP and DOX@CSP was investigated with or without 10 mM DTT. Typically, DOX@CCSP or DOX@CSP (10 mg) was dissolved under simulative physiological conditions in phosphate buffer (PBS, 2 mL) with or without 10 mM DTT. The solutions were then transferred to a dialysis bag (MWCO 3500). The drug release started once the dialysis bag was placed into a vial in which 8 mL of corresponding PBS were added. The vials were placed onto shaking tables and the temperature was maintained at 37 °C. At certain time intervals, 200 μL of dialysate was taken for DOX content analysis using a UV–vis spectrophotometer at 490 nm. The cumulative release rate of the drug from the loaded-nanocarriers was measured as the mass ratio of released drug compared to the loaded drug.

2.10. Hemolysis and biocompatibility assay

In order to further evaluate the biocompatibility of nanocarriers and hemolytic toxicity of nanocarriers and loaded nanocarriers, hemolysis and biocompatibility assays were carried out. To obtain red blood cells (RBCs), fresh goat blood was diluted in PBS (20:1, v/v) and centrifuged at 1500 rpm for 10 min. The supernatant was removed subsequently and the process was repeated until the supernatant became colourless. Afterwards, 10% v/v of the RBC suspension in PBS was obtained. 100 μL of various concentrations of DOX, nanocarriers and DOX@ nanocarriers were blended with 100 μL of the RBCs suspension on a 96-well plate which was later incubated in a cell incubator for 1.5 h. Meanwhile, 1% of Triton X-100 was used for complete hemolysis as positive control and PBS was used as negative control. After incubation, the supernatant was moved to a homologous location of another 96-well plate after centrifugation at 1500 rpm for 10 min. The absorbance at 540 nm was determined using a microplate reader (Thermo Scientific™ Multiskan™ FC). The hemolysis rate was measured using the following equation:

$$\text{Hemolysis}\% = \frac{OD_{sample} - OD_{negative\ \ control}}{OD_{positive\ \ control} - OD_{negative\ \ control}} \times 100$$

Where 1% of Triton X-100 was used for complete hemolysis as positive control and PBS was used as negative control.

Skov3 and HEK293T cells were cultured using RPMI-1640 and DMEM supplemented with 10% FBS at 37 °C with 5% CO_2 in a humidified incubator, respectively. The biocompatibility assay was determined using a CCK-8 assay. Firstly, Skov3 and HEK293T cells were cultivated in a 96-well plate (8000 cells per well) and incubated for 24 h. Afterwards, the culture medium was replaced with new medium containing varying concentrations of CCSP and CSP micelles. Then, the cells were incubated for another 24 h and a CCK-8 assay (10 μL) was introduced. Simultaneously, a CCK-8 assay (10 μL) with 90 μL nutrient solution was introduced into the blank wells without cells as a control group. After the cells were incubated for 2 h, the absorbance at 450 nm was measured through a microplate reader. The cell viability rate was calculated as follows (data were expressed as average ± SD (n = 6)):

$$\text{Cell viability rate} = \frac{OD_{sample} - OD_{control}}{OD_{blank} - OD_{control}} \times 100$$

Where sample, control and blank refer to the cells treated with varying concentrations of CCSP and CSP micelles, the untreated cells and culture medium without cells.

2.11. Cellular uptake of CCSP and CSP

The loading process of Coumarin-6 (C6) in CCSP or CSP was carried out following a similar procedure as described for Dox loading. Skov3 and HEK293T cells were cultivated on a 96-well plate (8000 cells per well) and incubated for 24 h. In order to further explore the controlled release performance towards glutathione (GSH, an antioxidant specifically elevated in tumor tissue), the cells were pretreated with BSO (250 μM, inhibitor of GSH) and GSH (5 mM) before addition of C6@CCSP and C6@CSP. Then, the cell nuclei and GSH were stained with Hoechst 33342 (C1025, Beyotime) and thioltracker (T10095, Thermo Fisher Scientific) for 30 min, respectively. Fluorescence images were recorded by an Operetta High-Content Imaging System. A flow cytometer was used to quantify the cellular-uptake of CCSP and CSP. SKOV3 and HEK293T cells were cultivated on a 6-well plate. Then, C6@CCSP and C6@CSP along with BSO and GSH were added to the cell culture similarly to the method described above. For another 2 h, the cells were collected and the fluorescence intensity of C6 was measured by flow cytometer.

2.12. In vivo antitumor efficiency of CCSP and CSP

Skov3 and HEK293T cells were cultivated on a 96-well plate (5000 cells per well) and incubated for 24 h. Afterwards, the nutrient medium was updated with fresh nutrient medium containing varying concentrations of DOX, DOX@CCSP or DOX@CSP (equivalent DOX concentration). After another 36 h of incubation, CCK-8 assay (10 μL) solution was added to each well. The absorbance at 450 nm was recorded using a microplate reader after another 2 h of incubation.

2.13. In vivo antitumor efficiency

Female BALB/c nude mice (18 ± 3 g, 4 weeks old) were purchased from Hunan Silaike Experimental Animal Co. Ltd. The approval number of the mice was SYXK 2016-0002. The nude mice were fed at the department of laboratory animals, Central South University. All animal experiments were carried out in accordance with regulations of the Institutional Committee for the Care and Use of Laboratory Animals in cancer research.

2.13.1. Tumor formation in nude mice

SKOV3 cells (200 μL, 5×10^6 cells ml^{-1} in PBS) were injected subcutaneously under the front legs of nude mice for tumor formation. The body weight and tumor volume were recorded every three days thereafter. The tumor volume was obtained through the formula as follows: V = (length × [width]^2)/2, where length and width stand for the longest and shortest diameter, respectively. When the tumor volume reached about 50 mm^3 in size, the mice were randomly divided into four groups (n = 6) for subsequent antitumor efficiency assays. Two animals were used for *in vivo* imaging studies.

2.13.2. In vivo imaging study

1,1-Dioctadecyl-3,3,3,3-tetramethylindotricarbocyanine iodide (Dir), a kind of NIR fluorescent dyes, was used to study the distribution of CCSP and CSP *in vivo*. CCSP or CSP loaded with Dir (Dir@CCSP or Dir@CSP) were synthesized similar to the method described for the synthesis of DOX@CCSP. Two mice were injected *via* tail vein injection with Dir@CCSP and Dir@CSP, respectively. After the mice were narcotized with isoflurane, the fluorescence intensity and distributions were recorded using a multi spectral imaging system. Finally, the mice were dissected, and fluorescence images of the main organs as well as the tumors were recorded using a multi spectral imaging system.

2.13.3. In vivo antitumor efficiency assay

The four groups of mice were administered with 200 μL saline solution (as the blank control), free DOX, DOX@CCSP, or DOX@CSP every three days, respectively. Before injection, the same amount of DOX in each solution was confirmed in each injection except for the blank control. Before injection, the body weight and tumor volume were recorded to assess the antitumor effect and any potential side effects of the treatments.

2.13.4. Distribution of DOX in nude mice

To explore the distribution of DOX in main tissues of nude mice, the mice were dissected after about three weeks of treatment. Then, the tumor tissues and major organs were weighed, grinded, extracted by chloroform, evaporated by vacuum-rotary, dissolved in chromatographic MeOH, ultrafiltered, and subjected to HPLC analysis. The corresponding drug was dissolved in 1 mL of the mobile phase (0.01 M KH_2PO_4: acetonitrile: acetic acid = 44:55:0.2 (V:V:V)) for subsequent HPLC analysis. The flow rate was 1 mL/min and the detection wavelength was set to 490 nm. The column parameters were: Agilent SB-C18, 4.6 × 150 mm diameter, 5 μm packing size.

2.13.5. Histological analysis with ematoxylin and eosin staining (H&E)

Samples of major organs and tumor were fixed in 4%

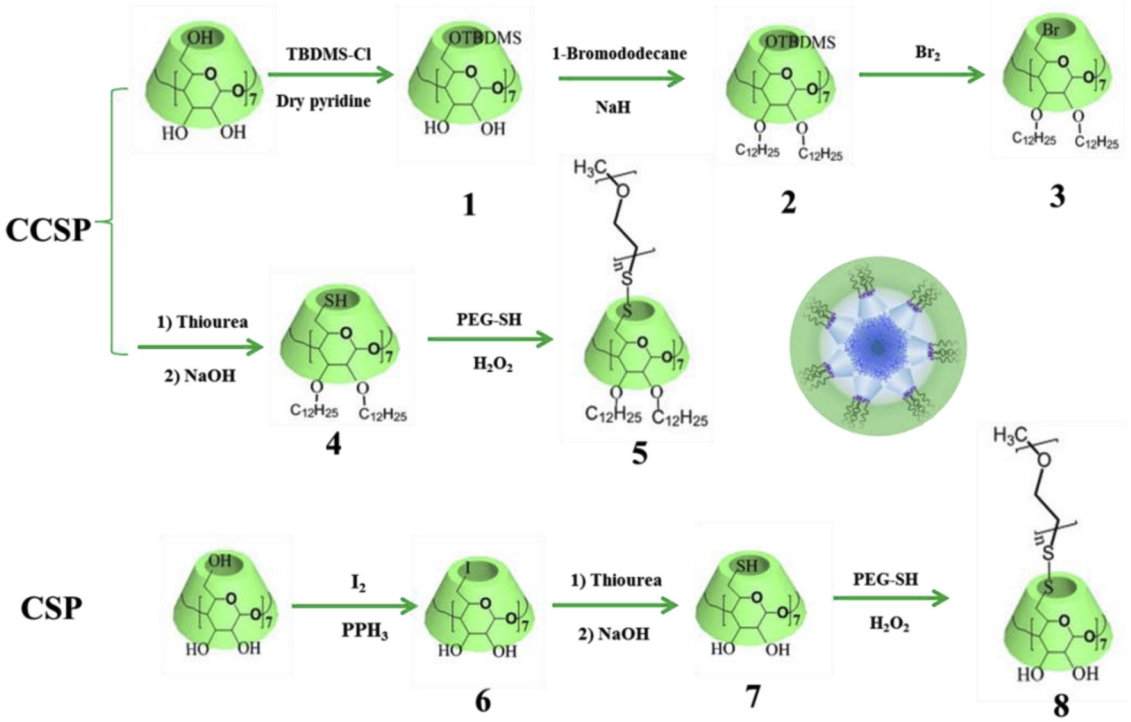

Scheme 1. Detailed synthetic procedure of CCSP and CSP.

paraformaldehyde, dehydrated, embedded in paraffin, cut into slices of 5 μm, dewaxed, HE dyed, and analyzed using a fluorescence microscope.

2.13.6. Terminal deoxynucleotidyl transferase biotin-d UTP nick end labeling (TUNEL) assay

TUNEL is a method to detect DNA apoptosis [26]. The detection method was employed to evaluate the anticancer effects of DOX, DOX@CCSP and DOX@CSP. This experiment was carried out using a TUNEL *in situ* Cell Death Detection Kit (Roche Diagnostics, Mannheim, Germany). Briefly, the tumor was fixed, embedded in paraffin, installed on glass slides, dewaxed, rehydrated, treated with proteinase K, dyed with TUNEL, and analyzed using a fluorescence microscope.

3. Results and discussion

3.1. Characterization of a series of synthetic intermediates

The preparation routes of CSSP and CSP are illustrated in Scheme 1. The compounds **1–8** were characterized using ^{1}H NMR and ^{13}C NMR spectroscopy (see Supporting information section) and FTIR. As shown in Figs. S3 and S5 (^{1}H NMR spectrum of compound **1**), two new peaks at 0.01, 0.84 ppm appeared and the peak at 4.45 ppm disappeared, which verified the successful functionalization of *tert*-butyldimethylsilyl on the primary hydroxyl groups. For compound **2** (Fig. S6), a new peak at 1.21 ppm, corresponding to the dodecyl group, appeared. Furthermore, the peak at 5.77 ppm, corresponding to the second hydroxyl groups of β-CD, disappeared. As shown in Fig. S8, the disappearance of the peak at 0.01 ppm and the reduction of the peak at 0.84 ppm provided evidence for the successful synthesis of compound **3**. As shown in Fig. S10, the appearance of a peak at 2.10 ppm, corresponding to −SH, confirmed that the bromide group was successfully replaced with thiol to form compound **4**. As shown in Fig. S16, an intense signal corresponding to PEG appeared at about 3.66 ppm and the thiol signal at 2.10 ppm disappeared, which provided evidence for the successful formation of compound **5.** Furthermore, as shown in Fig. S18, the peak at 4.45 ppm, corresponding to the primary hydroxyl groups of β-CD, disappeared, providing evidence for the successful iodination reaction to form compound **6**. As shown in Fig. S19, the appearance of a new peak at 2.14 ppm, corresponding to a thiol group, confirmed that iodide was successfully replaced with thiol to form compound **7**. As shown in Fig. S20, an intense signal corresponding to PEG at about 3.45 ppm appeared and the thiol peak at 2.14 disappeared, providing evidence for the successful synthesis of compound **8**. The ^{13}C NMR spectroscopy are consistent to a series of compound (see Supporting information section).

Fig. 2A shows the FTIR spectra of a sequence of prepared products. After protection of the primary hydroxyl groups in β-CD with *tert*-butyldimethylsilyl (Fig. 2A(b)), two new peaks at 1496 and 1360 cm^{-1} appeared, corresponding to −C−$(CH_3)_3$ bound to Si, as well as a new peak corresponding Si−$(CH_3)_2$ could be observed. The finding provided evidence for the successful introduction of *tert*-butyldimethylsilyl. As shown in Fig. 2A(c), the enhanced signals at 2823, 2924, 1463 cm^{-1}, exhibiting bonds stretching and deformation vibrations of $-(CH_2)_n-$, could be detected. This finding corresponded to the successful functionalization of the dodecyl group. As shown in Fig. 2A(d), after bromination, the peak at 1255 cm^{-1} disappeared, providing further evidence for the successful synthesis of $(C_{12}H_{25})_{14}$-β-CD-Br_7. Next, the appearance of a new peak at 2565 cm^{-1}, corresponding to -SH (Fig. 2A(e)), indicated a successful synthesis of $(C_{12}H_{25})_{14}$-β-CD-$(SH)_7$. As shown in curves (f) and (g), the peak at 2565 cm^{-1}, corresponding to -SH, disappeared and a peak at 1116 cm^{-1} corresponding to an asymmetric stretching vibration of C−O−C increased. This finding shows that PEG was successfully linked to β-CD *via* formation of a disulfide bond.

As shown in Fig. 2B, the SEM images show that CCSP exhibited a regularly spherical morphology, with a homogeneous diameter of about 40–50 nm and a distinct border. CSP (Fig. 2C) featured a spherical morphology, with a diameter of about 30–40 nm. The DLS (see Figs. S24–S27) showed that CCSP in PBS and cellular media had a diameter of about 200 nm. And CCSP had no obvious change after 10 days, which proved its good stability to some extent. However, the distribution of CSP had a great change especially in cellular media, which may result from the instability and bonding with proteins for CSP in cellular

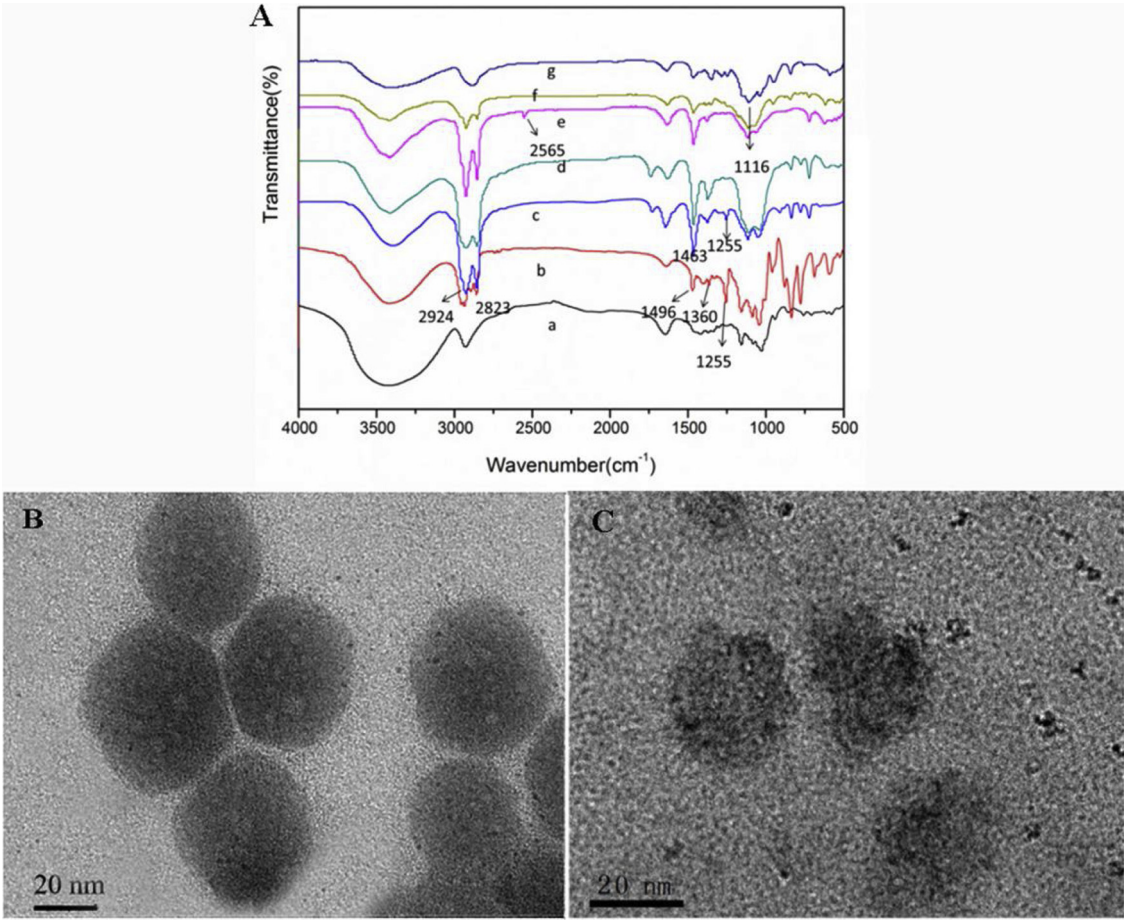

Fig. 2. (A) FTIR spectrum of a sequence of products (a: β-CD; b: β-CD-(OTBDMS)$_7$; c: $(C_{12}H_{25})_{14}$-β-CD-(OTBDMS)$_7$; d: $(C_{12}H_{25})_{14}$-β-CD-Br$_7$; e: $(C_{12}H_{25})_{14}$-β-CD-(SH)$_7$; f: $(C_{12}H_{25})_{14}$-β-CD-(S-S-PEG-OCH$_3$)$_7$ and g: β-CD-(S-S-PEG-OCH$_3$)$_7$). TEM images of (B) CCSP and (C) CSP.

media. Furthermore, It showed that CCSP and CSP could self-assemble in water. For CCSP, the hydrophobic core was formed by dodecyl groups and polyethylene glycol served as hydrophilic shell. For CSP, the hydrophobic core was formed by β-CD (the water solubility of β-CD was poorer than that of PEG) and PEG served as hydrophilic shell. Moreover, the energy spectra of CCSP and CSP, as shown in Figs. S22 and S23, provided further evidence for the successful synthesis of CCSP and CSP. The GPC measurement was conducted to obtain the relative molecular weights of CCSP and CSP (Fig. S28), which showed that the MW (weight-average molecular weight) were 16108 Da (PDI = 1.171) and 14021 Da (PDI = 1.017), respectively. It could prove the successful synthesis of CCSP and CSP to a certain degree.

3.2. Drug loading and drug release studies

According to UV spectrometry results obtained, the loading ratio of DOX in CCSP and CSP was 39.6 wt% and 21.4 wt%, respectively. To further explore the GSH-responsive release of DOX from DOX@CCSP and DOX@CSP, dithiothreitol (DTT) was used to simulate the intracellular environment in cancer. As shown in Fig. 3, a low cumulative release rate of DOX from DOX@CCSP in PBS could be observed without DTT (curve d), and only 23% of DOX was released after 103 h. On the contrary, the cumulative release rate of DOX from DOX@CCSP in PBS with DTT reached over 50% within 9 h (curve a). This finding was mainly due to the rapid cleavage of disulfide bonds and the disassembly of CCSP in the reductive microenvironment, whereas the disulfide bonds proved to be relatively stable in a non-reductive environment. On the contrary, the cumulative release rate of DOX from DOX@CSP in PBS with DTT (curve b) was similar to that of DOX@CCSP with DTT (curve a). However, the cumulative release rate of DOX from DOX@CSP in PBS without DTT (curve c) was found to be increased compared to that of DOX@CCSP without DTT (curve d). This latter finding may be attributed to drug leakage from DOX@CSP in this non-reductive environment. As expected, DOX@CCSP exhibited an excellent and fast release

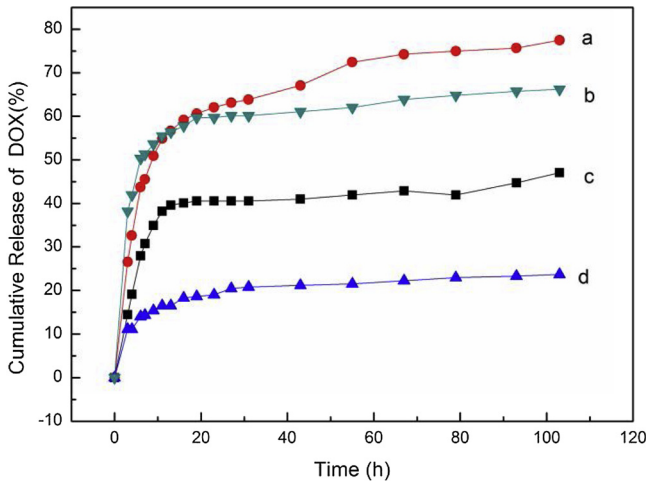

Fig. 3. DOX release curves from DOX-loaded CD nanoparticles in different media (a: DOX release curves from DOX@CCSP in PBS with DTT; b: DOX release curves from DOX@CSP in PBS with DTT; c: DOX release curves from DOX@CSP in PBS without DTT; d: DOX release curves from DOX@CCSP in PBS without DTT).

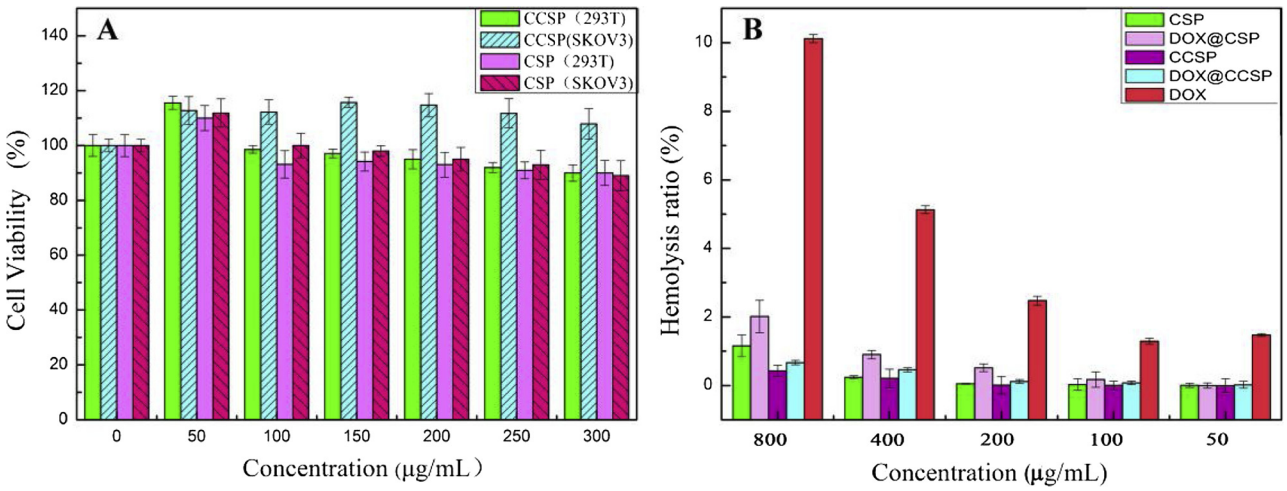

Fig. 4. (A) Viabilities of HEK293T and SKOV3 cells incubated with CCSP or CSP at different concentrations for 24 h, respectively; (B) Hemolytic test of CSP、DOX@CSP、CCSP or DOX@CCSP.

performance in a reductive environment and, moreover, showed low leakage in simulated blood circulation.

3.3. Biocompatibility in HEK293T and SKOV3 cells and hemolytic analysis

In order to estimate the biocompatibility of CCSP and CSP, the viabilities of HEK293T and SKOV3 cells cultured with CCSP or CSP at different concentrations and incubation for 24 h were measured. As shown in Fig. 4(A), even when the concentration of CCSP or CSP was up to 500 μg/mL, the viabilities of HEK293T and SKOV3 cells remained over 85%. This results explain that the prepared CCSP and CSP exhibited low toxicity to both HEK293T and SKOV3 cells and may therefore be considered promising to find use as carrier materials in clinical practice.

As shown in Fig. 4(B), the hemolytic toxicity of the carrier materials and the DOX-loaded system were below 2%. When the concentration reached up to 800 μg/mL, the hemolysis rate of CCSP or DOX@CCSP was below 0.8%, far below the international standard (5%), while the hemolysis rate of DOX@CSP was higher than that of DOX@CCSP, resulting from drug leakage from DOX@CSP without stimulation. The results indicate that CCSP exhibited hardly any hemolytic toxicity to RBC and could therefore be classified suitable for the use as a carrier material in clinical applications.

3.4. Intracellular drug release of C6@CCSP and C6@CSP

In order to analyze the cellular uptake of CCSP and CSP and the intracellular release of the drug, a green fluorescence probe-C6 was used to label CCSP and CSP. Moreover, Hoechst 33258 (blue) was employed to stain the nuclei, and a thioltracker (purple) was used to track GSH and thiol groups resulting from disulfide cleavage and dissociation on CCSP and CSP. As shown in Fig. 5A, an intense green and bright purple fluorescence could be observed in SKOV3 cells treated with C6@CCSP or C6@CSP without BSO or GSH. This latter finding verified that C6 could be released from C6@CCSP or C6@CSP in SKOV3 cells. When GSH was added to the system, the green and purple fluorescence of the SKOV3 cells increased, indicating that the release of C6 increased with the increase of intracellular GSH content. After BSO was added, the green and purple fluorescence of SKOV3 cells was found to be reduced due to the BSO inhibiting secretion of GSH. Meanwhile, after BSO was added, the green and purple fluorescence of the SKOV3 cells after incubation with CCSP was found to be weaker than that of CSP, resulting from the less C6 leaked from C6@CCSP in this non-reductive environment. As for the HEK293T cells, a very weak green fluorescence and a weak purple fluorescence could be observed in the HEK293T cells, which were treated with C6@CCSP or C6@CSP in the absence of BSO or GSH. This latter finding indicated that C6 could be released from C6@CCSP or C6@CSP, specifically in SKOV3 cells compared to HEK293T cells. This further demonstrated the high potency of DOX@CCSP to find use as a potential anticancer drug. In conclusion, C6 was found to be released both from C6@CCSP and C6@CSP in SKOV3 cells selectively, while only negligible C6 was found to be leaked from C6@CCSP in HEK293T cells. Therefore, CCSP proved to be more suitable than CSP as a carrier for a hydrophobic anticancer drug.

Flow cytometry was employed to quantify the cellular uptake of C6@CCSP and C6@CSP and the release of C6. The corresponding results were shown in Fig. 5B. We showed that the fluorescence intensity could be significantly enhanced when increasing the GSH content, and the fluorescence intensity in SKOV3 cells was far stronger than that in HEK293T cells without BSO or GSH. This latter finding was consistent with the results obtained from fluorescence images and the results further verified that C6 could be released from C6@CCSP in SKOV3 cells selectively. Taken in concert, DOX@CCSP indeed showed characteristics promising to enhance the anticancer effect with reduced side effects towards normal cells.

3.5. Cytotoxicity studies

It is significant to assess the cytotoxicity of DOX@CCSP and DOX@CSP. Through a CCK-8 assay, the half-maximal inhibitory concentration (IC_{50}) was employed as a means to assess the DOX cytotoxicity to normal HEK293T cells and cancerous SKOV3 cells. As shown in Fig. 6, free DOX exhibited significant toxicity to both HEK293T and SKOV3 cells, with an IC_{50} value of ˜0.8 μg/mL and 1.0 μg/mL, respectively. DOX@CCSP and DOX@CSP also exhibited a strong cytotoxicity to SKOV3 cells, but showed weak cytotoxicity towards HEK293T cells. The IC_{50} value of DOX@CCSP and DOX@CSP at an equivalent DOX concentration was 2.0 μg/mL and 1.0 μg/mL against SKOV3 cells and over 12 μg/mL and ˜12 μg/mL against HEK293T cells, respectively. When the concentration of DOX was 5.0 μg/mL, the observed viability of SKOV3 cells and HEK293T cells was about 32%, 80% upon treatment with DOX@CCSP and 40%, 68% after treatment with DOX@CSP, respectively. Therefore, at a DOX concentration of 5.0 μg/mL, DOX@CCSP exhibited high cytotoxicity towards SKOV3 cells and showed no obvious damaging effects towards HEK293T cells. However, DOX@CSP showed a lower efficacy and more severe side effects compared to DOX@CCSP which may be a result of the DOX leakage from DOX@CSP under normal physiological conditions. The cytotoxicity results demonstrated the excellent anticancer efficacy and low side effects of DOX@CCSP, most likely resulting from the high loading

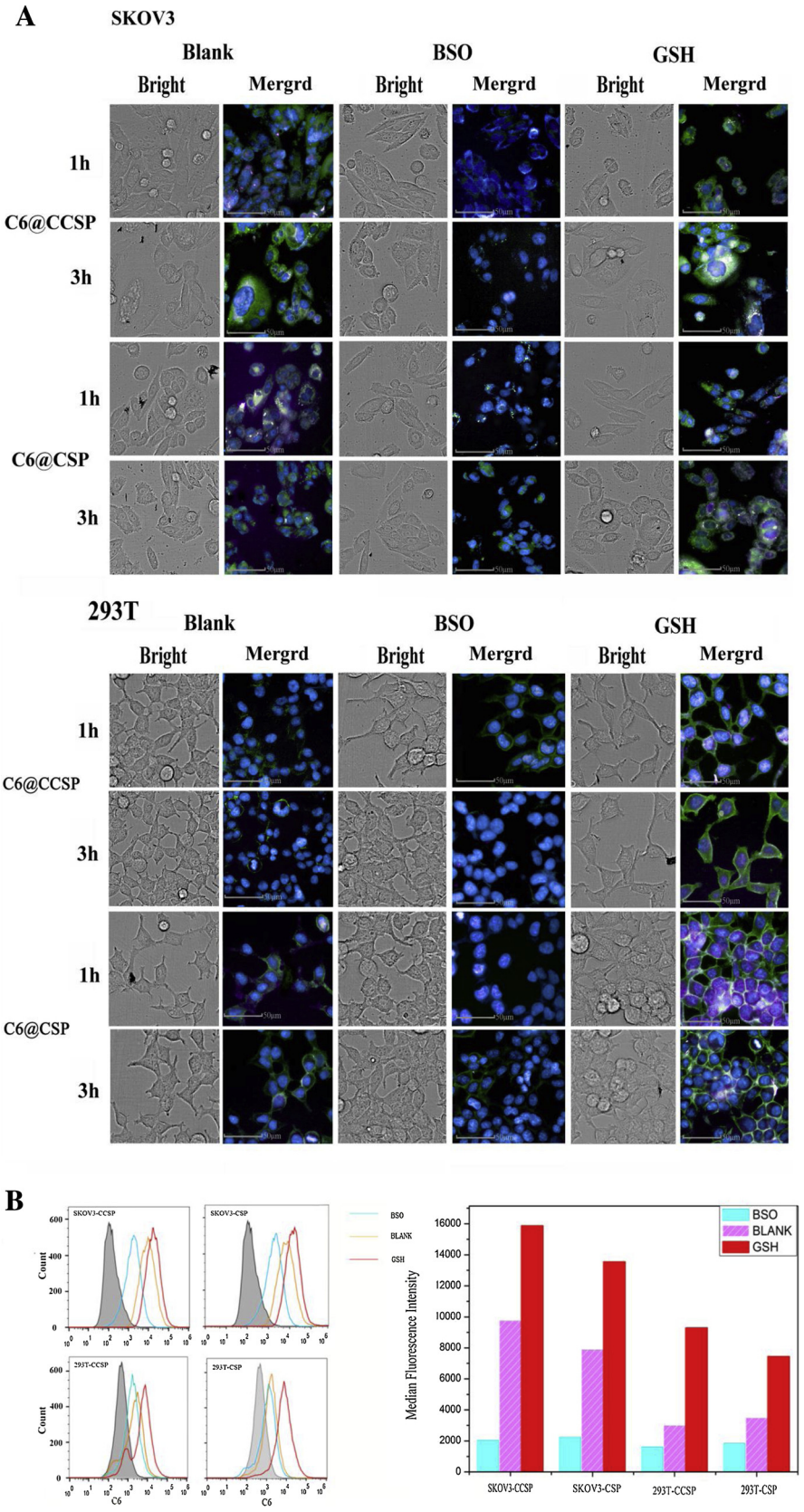

Fig. 5. (A) Fluorescence images of SKOV3 and HEK293T cells after incubation with C6@CCSP and C6@CSP for 1 h and 3 h, respectively; (B) Cellular uptake and median fluorescence intensity of C6@CCSP and C6@CSP in SKOV3 and HEK293T cells by flow cytometry.

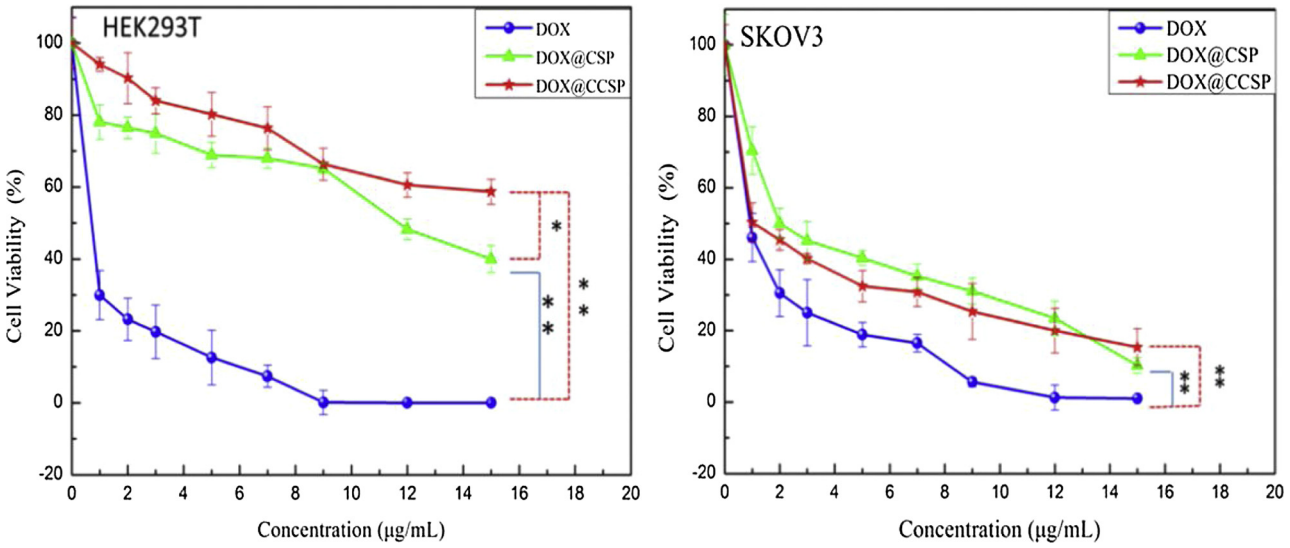

Fig. 6. Cytotoxicity studies for HEK293T and SKOV3 cells cultured with DOX, DOX@CSP and DOX@CCSP at different concentrations for 24 h (*p < 0.05,**p < 0.01).

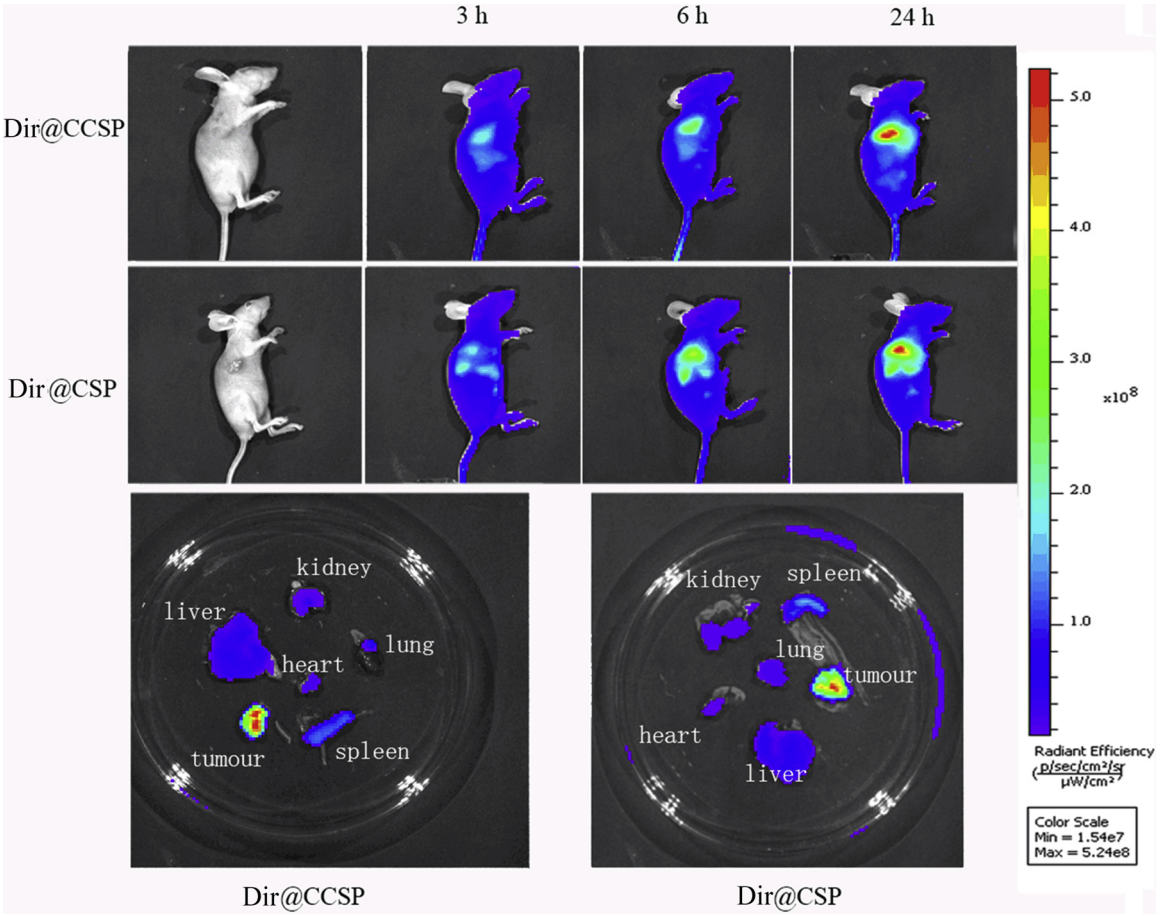

Fig. 7. Biodistribution of Dir@CCSP and Dir@CSP in mice bearing SKOV3 tumors for different time periods and biodistribution in major tissues and tumor at 24 h.

capacity, superior stimuli-responsive release properties, low leakage and suitable particle size.

To further study the cellular uptake and cytotoxicity properties, the cells were incubated with DOX@CCSP, DOX@CSP and DOX for 36 h and exhibited fluorescence. As shown in Figs. S29–S31, when the concentration of DOX was 5 μg/mL, DOX@CCSP, DOX@CSP and DOX exhibited a strong red fluorescence and high cytotoxicity toward SKOV3 cells and the nuclei of SKOV3 cells were found to be damaged to varying degrees. Due to the poor adhesion of 293T cells, dead cells would fall out, therefore most remaining 293T cells were found to be undamaged, and the decrease of 293T cells would result from increasing cytotoxicity. As shown in Figs. S32–S34, at a DOX concentration of 5 μg/mL, DOX@CCSP exhibited low cytotoxicity towards 293T cells. These results demonstrated the excellent anticancer performance

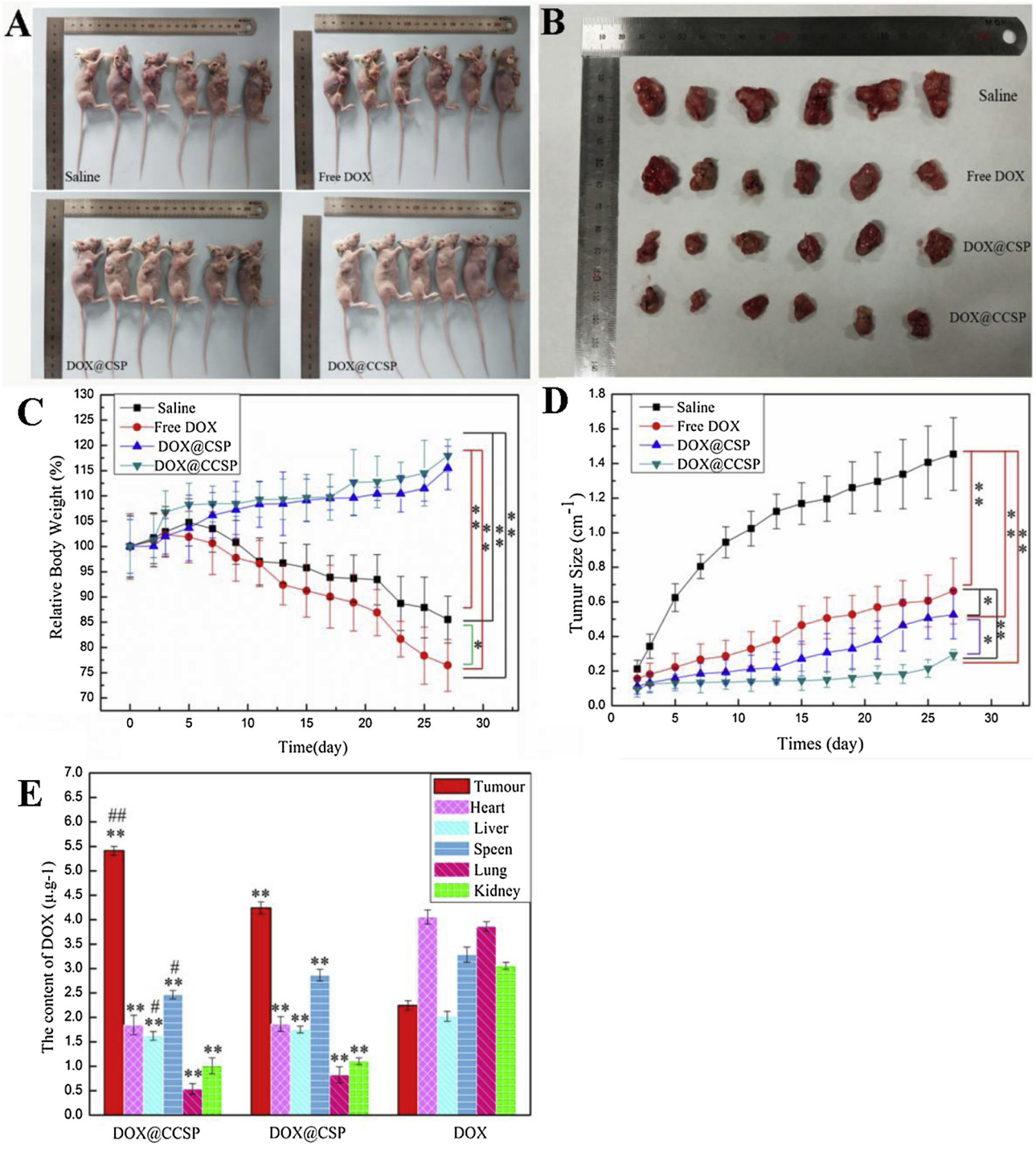

Fig. 8. (A) Photographs of mice after treatment with saline, DOX, DOX@CSP, DOX@CCSP for 27 days. (B) Body weight changes of mice during treatment with saline, DOX, DOX@CSP or DOX@CCSP. The body weights were normalized to the initial values (*P < 0.05 and **P < 0.01). (C) Photographs of tumor after treatment with saline, DOX, DOX@CSP or DOX@CCSP for 27 days. (D) Relative tumor volume changes of tumors in mice during the treatment with saline, DOX, DOX@CSP or DOX@CCSP. (*P < 0.05 and **P < 0.01). (E) Concentration of DOX in tumor tissues and major organs in mice after treatment by HPCL. (*P < 0.05 and **P < 0.01 *versus* free DOX group, $^{\#}$P < 0.05 and $^{\#\#}$P < 0.01 *versus* DOX@CSP group).

and low side effects of DOX@CCSP, consistent with the results described above.

3.6. *In vivo* biodistribution

Two mice were injected with Dir@CCSP and Dir@CSP *via* tail vein injection, respectively. Then, the mice were imaged *via* an IVIS Lumina II multispectral imaging system for 3, 6 and 24 h. As shown in Fig. 7, the fluorescence of Dir@CCSP and Dir@CSP was accumulated in the tumor sites with time due to the EPR effect, favourable stimuli-responsive properties and suitable particle size. After 24 h of imaging, the tumors and main tissues were extracted for imaging. The results obtained indicate that strong fluorescence could only be detected in tumor tissue, while no obvious significant fluorescence could be detected in the main tissues. However, the fluorescence intensity of Dir@CCSP in the main tissues was weaker than that of Dir@CSP, mainly due to the

drug leakage of Dir@CSP in blood circulation. The suitable size and favourable stimuli-responsive properties led to accumulation and release of Dir@CCSP in tumor tissues while the low drug leakage of CCSP may benefit to decrease side-effect in normal tissues.

3.7. Antitumor efficacy of DOX@CCSP and DOX@CSP in vivo

The mice were divided into four groups. And each group of animals were injected with saline, free DOX, DOX@CSP and DOX@CSSP, respectively. As shown in Fig. 8, the relative body weights and the tumor sizes were recorded. Mice in the saline group exhibited an obvious decrease in body weight and a distinct increase in tumor size over time. The loss in body weight mainly resulted from the fact that the tumors were too large for the mice to bear. As for the mice in the other three groups, the tumor sizes were significantly smaller compared with those in the saline group, particularly in the DOX@CCSP groups. This latter finding provides more evidence for the outstanding anticancer efficacy of DOX@CCSP due to the EPR effect and favourable stimuli-responsive properties. However, the body weights in the DOX group decreased over time and the mice were skinny after therapy for 27 days due to the severe side effects of DOX. The body weights in DOX@CCSP group increased gradually due to the low side effect resulting from the low DOX leakage in normal tissues. As described above, DOX@CCSP showed excellent anticancer efficacy and reduced toxicity to normal tissues *in vivo*.

The concentration of DOX in tissues and tumors were quantified by HPLC. As shown in Fig. 8E, the DOX concentration in tumor tissues for the DOX@CCSP group was 2.2 times greater than that of the free DOX group. Meanwhile, in the DOX@CCSP group, the DOX concentration in tumor tissues was more than twice of that in normal tissues. Here, DOX@CCSP mainly benefited from the EPR effect and superior stimuli-responsive release properties. Furthermore, in the free DOX group, the DOX concentrations in normal tissues were higher than the concentration in tumor tissues. This latter finding was the main reason causing significant toxicity to normal tissues.

Histopathological analysis was performed to assess potential damages to normal tissues and tumor tissues caused by DOX, DOX@CCSP or DOX@CSP. As shown in Fig. S34-A, compared to the free DOX group, no obvious damages were observed in the main tissues of the heart, liver, spleen, lung and kidney in the DOX@CCSP and DOX@CSP groups. Particularly for the DOX@CCSP, the damages to normal tissues were similar to the saline group due to the EPR effect, superior stimuli-responsive release properties and negligible drug leakage. The tumor tissues after treatment with DOX@CCSP exhibited significant damages compared to the free DOX group. This latter finding was most likely due to the accumulation of DOX in tumor tissues, resulting in an improved anticancer efficacy. Moreover, a TUNEL assay was carried out to detect tumor cell apoptosis, as shown in Fig. S34-B. Green fluorescence indicated the varying levels of cell apoptosis. As shown here, compared to the free DOX group, a stronger green fluorescence could be observed in tumor tissue after treatment with DOX@CCSP and DOX@CSP compared to that treated with free DOX. DOX@CCSP in particular exhibited a superior anticancer efficacy. Taken in concert, the list of results confirmed that the DOX@CCSP system featured an outstanding anticancer effect and low side effects.

4. Conclusions

In summary, we have designed a new amphiphilic star-like diblock copolymer as a delivery platform for anticancer drug based on β-CD derivatives. The amphipathic β-CD was synthesized by chemical bonding in order to retain the nature cavity of β-CD and in an effort to increase the drug loading content. The corresponding intermediates and amphiphilic β-CD copolymer were characterized using ^{1}H NMR spectroscopy, ^{13}C NMR spectroscopy and FTIR. The CCSP could self-assemble into a regular spherical shape in water. In this medium, the dodecyl acted as hydrophobic core and the polyethylene glycol served as hydrophilic shell, where the cavity of β-CD and the hydrophobic cavity of the self-assembled material provided a suitable area to load DOX, with a drug loading content as high as 39.6 wt%. Drug-release analysis *in vitro* under simulated tumor environments provided evidence for the excellent performance for drug controlled-release. The results obtained from cellular experiments demonstrated that CCSP were biocompatible and DOX@CCSP could selectively destroy cancerous SKOV3 cells, however, exhibited low toxicity towards normal HEK293T cells. Moreover, the experimental results *in vivo* showed that DOX@CCSP could accumulate and release in tumorous tissue and revealed a suitable anticancer effect and very low side effects in normal tissues of tumor-bearing nude mice. Benefiting from the advantages of DOX@CCSP nanocarriers such as proper size, high loading content, favourable stimulus-response release performance and low drug leakage, it is believed that DOX@CCSP may potentially be used as an intelligent nanocarrier system for efficient anticancer drug delivery.

Author contributions

S.Z. and H.L. designed the study; H.L., J.C., X.L., Z.D. and J.L. carried out the synthetic route and characterization of the corresponding intermediates and amphiphilic β-CD copolymer; H.L. and T.R. performed the drug release studies; H.L., L.H., and Z.D. accomplished the cell experiments; H.L, J.C. and X.L. accomplished the animal experiments; Y.Y. provided significant advice for article writing; H.L. accomplished the manuscript. All authors have approved the final article.

Acknowledgments

The authors declare no competing financial interest. This study was funded by the National Natural Science Foundation of China (Grant No. 21576295), the Open-End Fund for the Valuable, Precision Instruments of Central South University (CSUZC201830) and the Fundamental Research Funds for the Central Universities of Central South University (2017zzts175 and 2018zzts371).

Appendix A. Supplementary data

Supplementary material related to this article can be found, in the online version, at doi:https://doi.org/10.1016/j.colsurfb.2019.05.011.

References

[1] M.J. Rohovie, M. Nagasawa, J.R. Swartz, Virus-like particles: next-generation nanoparticles for targeted therapeutic delivery, Bioeng. Transl. Med. 2 (2017) 43–57.
[2] Y. Hu, J. Chen, X. Li, Y. Sun, S. Huang, Y. Li, H. Liu, J. Xu, S. Zhong, Multifunctional halloysite nanotubes for targeted delivery and controlled release of doxorubicin in-vitro and in-vivo studies, J. Agric. Food Chem. 65 (2017).
[3] J. Chen, X. Li, J. Li, J. Li, L. Huang, T. Ren, X. Yang, S. Zhong, Assembling of stimuli-responsive tumor targeting polypyrrole nanotubes drug carrier system for controlled release, Mater. Sci. Eng. C 89 (2018) 316–327.
[4] C.G. England, H.J. Im, L. Feng, F. Chen, S.A. Stephen, R. Hernandez, H. Orbaye, C. Xu, S.Y. Cho, R.J. Nickles, Z. Liu, D.S. Lee, W. Cai, Re-assessing the enhanced permeability and retention effect in peripheral arterial disease using radiolabeled long circulating nanoparticles, Biomaterials 100 (2016) 101–109.
[5] J.B. Ten Hove, J. Wang, M.N. Oosterom, V.L. Fwb, A.H. Velders, Size-sorting and pattern formation of nanoparticle-loaded micellar superstructures in biconcave thin films, ACS Nano 11 (2017) 11225–11231.
[6] J. Chen, X. Li, Y. Sun, Y. Hu, Y. Peng, Y. Li, G. Yin, H. Liu, J. Xu, S. Zhong, Synthesis of size-tunable hollow nanostructures and their assembly into folate targeting and pH-responsive anti-cancer drug delivery, Chem.—Eur. J. 23 (2017) 17279–17289.
[7] H. Maeda, The enhanced permeability and retention (EPR) effect in tumor vasculature: the key role of tumor-selective macromolecular drug targeting, Adv. Enzyme Regul. 41 (2001) 189–207.
[8] S.S. Han, Z.Y. Li, J.Y. Zhu, K. Han, Z.Y. Zeng, W. Hong, W.X. Li, H.Z. Jia, Y. Liu, R.X. Zhuo, X.Z. Zhang, Dual-pH sensitive charge-reversal polypeptide micelles for tumor-triggered targeting uptake and nuclear drug delivery, Small 11 (2015) 2543–2554.
[9] X. Shi, X. Ma, M. Hou, Y.E. Gao, S. Bai, B. Xiao, P. Xue, Y. Kang, Z. Xu, C.M. Li, pH-Responsive unimolecular micelles based on amphiphilic star-like copolymers with high drug loading for effective drug delivery and cellular imaging, J. Mater. Chem.

B 5 (2017) 6847–6859.
[10] C. Yan, Z. Guo, Y. Shen, Y. Chen, H. Tian, W.H. Zhu, Molecularly precise self-assembly of theranostic nanoprobes within a single-molecular framework for in vivo tracking of tumor-specific chemotherapy, Chem. Sci. 9 (2018) 4959–4969.
[11] T. Sun, Y.S. Zhang, B. Pang, D.C. Hyun, M. Yang, Y. Xia, Engineered nanoparticles for drug delivery in cancer therapy, Angew. Chem. Int. Ed. 53 (2015) 12320–12364.
[12] M. De Smet, S. Langereis, S. Bosch, H. Grull, Temperature-sensitive liposomes for doxorubicin delivery under MRI guidance, J. Control. Release 143 (2010) 120–127.
[13] X. Meng, B. Gui, D. Yuan, M. Zeller, C. Wang, Mechanized azobenzene-functionalized zirconium metal-organic framework for on-command cargo release, Sci. Adv. 2 (2016) e1600480.
[14] S. Mura, J. Nicolas, P. Couvreur, Stimuli-responsive nanocarriers for drug delivery, Nat. Mater. 12 (2013) 991–999.
[15] Y. Yang, L. Xu, W. Zhu, L. Feng, J. Liu, Q. Chen, Z. Dong, J. Zhao, Z. Liu, M. Chen, One-pot synthesis of pH-responsive charge-switchable PEGylated nanoscale coordination polymers for improved cancer therapy, Biomaterials 156 (2018) 121–133.
[16] C. Hegedűs, K. Kovács, Z. Polgár, Z. Regdon, É. Szabóc, A. Robaszkiewicz, H.J. Forman, A. Martner, L. Virág, Redox control of cancer cell destruction, Redox Boil 16 (2018) 59–74.
[17] C. Sun, X. Li, X. Du, T. Wang, Redox-responsive micelles for triggered drug delivery and effective laryngopharyngeal cancer therapy, Int. J. Biol. Macromol. 112 (2018) 65–73.
[18] Z. Lyu, X. Shi, J. Lei, Y. Yuan, L. Yuan, Q. Yu, H. Chen, Promoting neural differentiation of embryonic stem cells using β-cyclodextrin sulfonate, J. Mater. Chem. B 5 (2017) 1896–1900.
[19] P. Mischnick, Determination of the patterns of substitution of hydroxyethyl and hydroxypropyl-cyclomaltoheptaoses, Carbohydr. Res. 192 (1989) 233–241.
[20] P.A. Faugeras, B. Boëns, P. Elchinger, F. Brouillette, D. Montplaisir, R. Zerrouki, R. Lucas, When cyclodextrins meet click chemistry, Eur. J. Org. Chem. 22 (2012) 4087–4105.
[21] R. Gref, M. Lück, P. Quellec, M. Marchand, E. Dellacherie, S. Harnisch, T. Blunk, R.H. Müller, 'Stealth' corona-core nanoparticles surface modified by polyethylene glycol (PEG): influences of the corona (PEG chain length and surface density) and of the core composition on phagocytic uptake and plasma protein adsorption, Colloid Surf. B 18 (2000) 301–313.
[22] Z. Quan, C. Ying, X.J. Wang, J.L. Xu, Z. Ye, S. Wang, Targeted photodynamic killing of breast cancer cells employing heptamannosylated β-cyclodextrin-mediated nanoparticle formation of an adamantane-functionalized BODIPY photosensitizer, ACS Appl. Mater. Interface 8 (2016) 33405–33410.
[23] H. Xiong, D. Zhou, X. Zheng, Y. Qi, Y. Wang, X. Jing, Y. Huang, Stable amphiphilic supramolecular self-assembly based on cyclodextrin and carborane for the efficient photodynamic therapy, Chem. Commun. 53 (2017) 3422–3425.
[24] Y. Shi, H. Li, J. Cheng, T. Luan, D. Liu, Y. Cao, X. Zhang, H. Wei, Y. Liu, G. Zhao, Entirely oligosaccharide-based supramolecular amphiphiles constructed via host-guest interactions as efficient drug delivery platforms, Chem. Commun. 53 (2017) 12302–12305.
[25] B. Nezha, J. Nathalie, G. Philippe, Synthesis of per-2,3-di-*O*-heptyl-β and γ-cyclodextrins: a new kind of amphiphilic molecules bearing hydrophobic parts, Tetrahedron Lett. 47 (2006) 8925–8927.
[26] P. Ashton, K. Rainer, J. Stoddart, D. Alker, V. Harding, Amino acid derivatives of β-cyclodextrin, J. Org. Chem. 61 (2010) 903–908.
[27] Q. Zhang, G.Z. Li, C.R. Beser, D.M. Haddleton, Cyclodextrin-centred star polymers synthesized via a combination of thiol-ene click and ring opening polymerization, Chem. Commun. 48 (2012) 8063–8065.
[28] F. Saadati, H. Mahdikia, H.A. Abbaszadeh, M.A. Abdollahifar, M.S. Khoramgah, B. Shokri, Comparison of direct and indirect cold atmospheric-pressure plasma methods in the B16F10melanoma cancer cells treatment, Sci. Rep.—UK 8 (2018), https://doi.org/10.1038/s41598-018-25990-9.